Experimental Study on Seismic Behavior of Q620E High-strength Steel Box-section Columns with Low Yield Ratio

Xiyu Ye [1], Shidong Nie[1,*], Zhenye Chen [2], Cheng Ma [2], and Jin Pan [2]

[1] School of Civil Engineering of Chongqing University, Chongqing, China
[2] User Technology Center of Materials Technology Research Institute of HBIS, Hebei, China
Email: 20164934@cqu.edu.cn (X.Y.); nieshidong@cqu.edu.cn (S.D.N.); chenzhenye@hbisco.com (Z.Y.C.); macheng01@hbisco.com (C.M.); panjin@hbisco.com (J.P.)
*Corresponding author

***Abstract*—The high yield ratio of high-strength steel limits its application in the seismic design of members. China HBIS Group has developed a new kind of low yield ratio steel Q620E to address this problem. The seismic performance test has been conducted on box-section columns made of such steel, and specimens with different cross-sectional dimensions were designed and subjected to low cyclic loading test under axial pressure. The seismic performance of the specimens was analyzed in terms of bearing capacity, energy consumption and damage development by observing the damage mode, extracting hysteresis curve and skeleton curve. The test results were compared with Q690D high-strength steel box-section columns. It shows that the low yield ratio high-strength steel box-section columns have good hysteresis performance and plastic deformation capacity; the larger the width to thickness ratio of the plate is, the more discontinuous the damage development is. This type of low yield ratio steel shows greater advantages than Q690D high-strength steel in mechanical properties and seismic design of members. It may be considered for extended applications in steel frame building.**

***Keywords*—high-strength steel, low yield ratio, box-section column, seismic behavior, low cyclic loading test**

I. Introduction

The requirements of building structures for steel performance are increasing. The use of high-strength steel can effectively reduce the weight of the structure itself, reduce the consumption of materials and promote energy-saving and environmentally friendly economic building construction [1]. However, the high yield ratio of steel usually reduces its plastic deformation capacity, which limits the application of seismic design.

Several scholars have conducted research on the seismic behavior of high-strength steel welded columns. The experiments were mainly conducted for Q460 and Q690 steel. Hysteresis tests and finite element fitting are used to summarize the factors influencing the seismic performance of the members [2–4]. Based on the hysteresis curves extracted from the tests, a polyline model was summarized to describe the moment-curvature relationship of steel columns [5]. On this basis, the influence of cyclic degradation on the model is considered. The two damage dominant modes, local buckling and low circumferential fatigue, are proposed to establish the cyclic degradation hysteresis model [6–7]. It can be seen that the research work on high-strength steel columns has started recently, and the yield ratio of high-strength steel grades larger than Q460D is generally larger than 0.9, which does not meet the steel material property requirements for seismic design of Chinese codes.

In response to the problem that the yield ratio of high-strength steel is generally higher than 0.9, China HBIS Group has developed a new kind of Q620E high-strength steel, which has a low yield ratio (around 0.85), good plastic deformation capacity and workability. In this paper, three box-section columns made of it were subjected to low cyclic test under axial pressure. Analyze its seismic performance and explore the feasibility of its seismic design.

II. Experimental Program

A. Material Properties

The specimens were taken from the 8mm thick Q620E steel plate produced by HBIS Group, China. The mechanical properties of the steel and the corresponding welding wire HS80GJ were tested. The data of elastic modulus E, yield strength f_y, tensile strength f_u, yield ratio f_y/f_u, ultimate strain ε_u, elongation after fracture δ and sectional elongation Z are recorded in Table I. The stress-strain curve of the steel is shown in Fig. 1. It can be seen

Manuscript received February 8, 2023; revised March 22, 2023; accepted May 25, 2023; published January 29, 2024.

doi: 10.18178/ijscer.13.1.1-6

that the new steel yield-strength ratio is lower than 0.9 and the elongation after fracture δ is greater than 16%, which satisfies the specification requirements of "Standard for design of high strength steel structure"[8].

TABLE I. MECHANICAL PROPERTIES OF Q620E HSS PLATE AND WELDING STICK-HS80GJ

-	E/MPa	f_y/MPa	f_u/MPa	f_y/f_u	ε_u	δ/%	Z/%
Q620E	210286	655.1	761.9	0.86	0.0753	22.5	65.9
HS80GJ	—	755.0	875.0	—	—	19.5	—

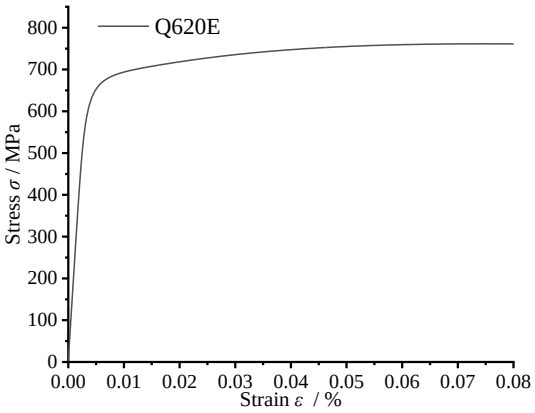

Fig. 1. Stress σ –strain ε relationship of Q620E steel.

B. Specimen Design

The dimensional information of the box-section columns is shown in Table II. D and t mean the width of the section and plate thickness respectively. The dimensions are labeled as shown in Fig. 2. L_0 is the calculated length of the suspended column, b_0/t is the width-thickness ratio of the plate. Level S2 indicates the finite plastic development section and level S4 indicates the elastic section. n is the nominal axial compression ratio.

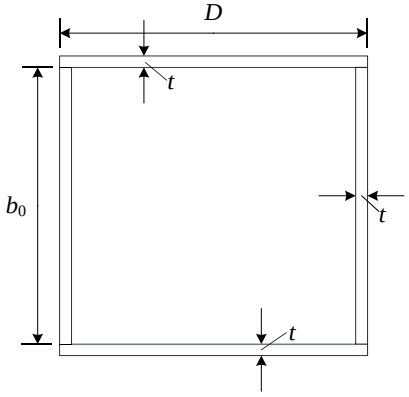

Fig. 2. Dimensions of box-section column.

TABLE II. DIMENSIONS OF BOX-SECTION COLUMNS

-	L_0/mm	D/mm	t/mm	b_0/t	n
B-1	1060	210	8	24.3(S4)	0.20
B-2	1060	180	8	20.5(S2)	0.20
B-3	1060	180	8	20.5(S2)	0.35

C. Test Setup and Instruments

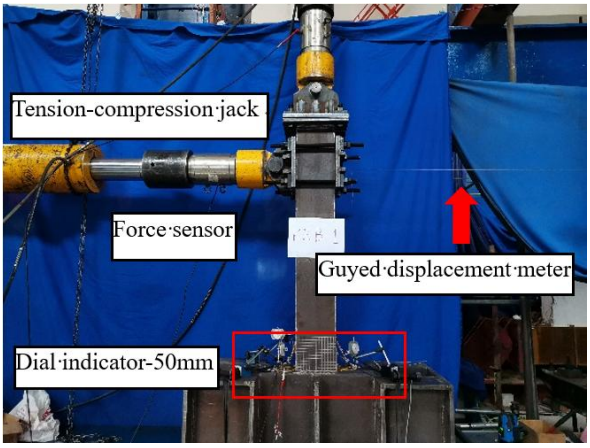

Fig. 3. Test loading device.

The test was conducted on the reaction frame in the structural engineering laboratory of Chongqing University. The loading device is shown in Fig. 3. The specimen is simplified as a cantilevered column with one end rigidly connected and the other end free. The horizontal load and axial pressure are provided by the 200-ton tension-compression jack. The bottom of the column is set up with a fully welded support to simulate a rigid base. The top of the column is connected with a pin to simulate the free end, and the horizontal load is applied to the proposed position of the counter-bending point. The guyed displacement meter is used to record the horizontal displacement of the column end and the dial indicator is used to estimate the curvature of the column bottom and monitor whether horizontal slippage of the bottom exists.

D. Loading Protocol

The axial pressure is held after the nominal axial pressure ratio is reached. The formal loading is carried out after the steel column is stabilized. The horizontal load is controlled by displacement. Take the horizontal displacement d_y as the displacement increment where the edge fiber reaches the yield state.

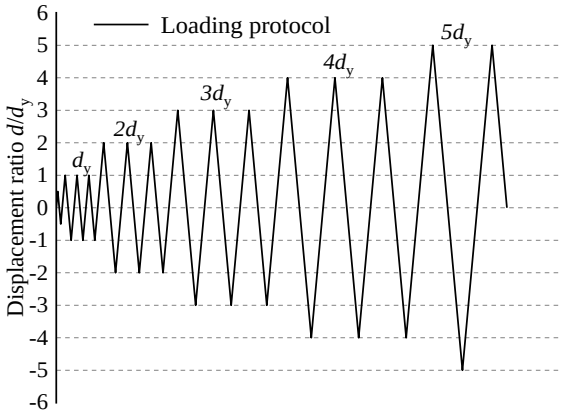

Fig. 4. Loading protocol.

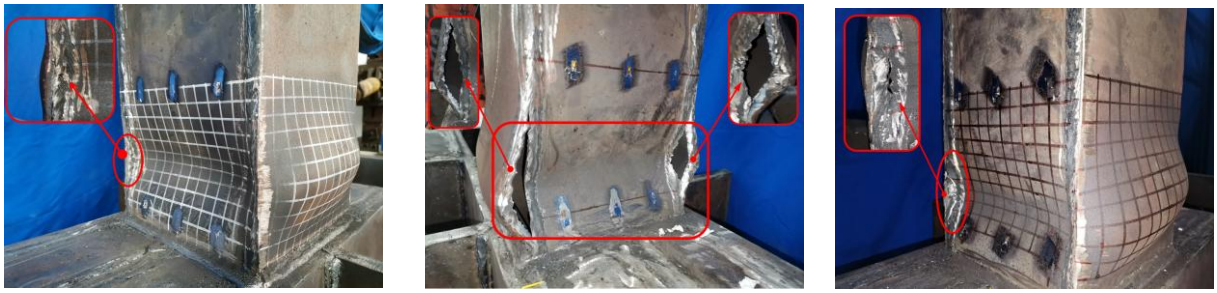

(a) B-1 (b) B-2 (c) B-3

Fig. 5. Failure modes of specimens.

Take step-by-step increments as loading levels. The loading protocol is shown in Fig. 4. After the section of the member enters the edge yield state, each stage of displacement is cycled at least 2 turns. When the specimen is loaded until the horizontal force falls below 85% of the peak load, the specimen is considered damaged.

III. Test Results and Discussion

A. Failure Modes

There is no obvious plate buckling phenomenon when the displacement of the end of column is loaded to d_y. With the increasing displacement, local buckling phenomenon can be observed on the bearing side of the wall plate, and finally the wall plate buckling of the column leads to the cracking of the weld. The weld fracture pattern of specimenis is detailed in Fig. 5. Excessive local buckling deformation of plate may lead to weld fracture. It is generally consistent with the expected phenomenon of the experiment. The records loading process is shown in Table III. The numbers in parentheses represent the circles in which the phenomenon occurred.

TABLE III. Test Observations of Specimens

Experimental phenomena	B-1	B-2	B-3
Yielding stage	$2d_y(1)$	$2d_y(1)$	$2d_y(1)$
Peak load-bearing stage	$3d_y(1)$	$3d_y(1)$	$3d_y(1)$
Local buckling of plate	$3d_y(1)$	$4d_y(1)$	$3d_y(2)$
Specimen failure	$3d_y(3)$	$4d_y(2)$	$4d_y(2)$

The main destruction mode of the specimen is local buckling of the plate and the fracture of the weld. By comparing specimen B-1 and B-2, it can be seen that, under the same nominal axial pressure ratio, the larger the aspect ratio is, the earlier the plat enters into local buckling state. Comparing specimen B-2 and B-3 with the same cross-sectional dimensions, B-3 with larger axial pressure enters the plate buckling state earlier.

B. Measured Hysteretic Curves and Analysis

Extract the hysteresis curve peak point to draw the skeleton curve, as shown in the Fig. 6. The hysteresis curves of bending moment M and horizontal displacement d are plotted in Fig. 7. The peak load M_u of all the specimens is greater than the yield bending moment M_y, which effectively utilizes the strength of the steel. The bearing capacity and ductility of B-2 and B-3 specimens are higher than that of B-1, which indicates that the influence of the width-thickness ratio on the bearing and plastic deformation capacity is obvious. The smaller the width-thickness ratio is, the higher the bearing performance and ductility are. The cross-sectional dimensions of B-2 and B-3 specimens are the same but the axial pressure ratio is different. The influence of the axial pressure ratio on the bearing capacity of the member may not be obvious. However, as the axial pressure ratio increases, the effect of gravity second-order effect increases and the maximum inter-story drift angle θ_u decreases. The results of hysteresis curve calculation are shown in the Table Ⅳ.

TABLE IV. Test Results of Hysteretic Curve

-	M_y/kN • m	M_u/kN • m	M_u/M_y	θ_u/%
B-1	292.7	349.2	1.19	4.18
B-2	210.6	339.1	1.61	5.51
B-3	210.6	352.2	1.67	4.61

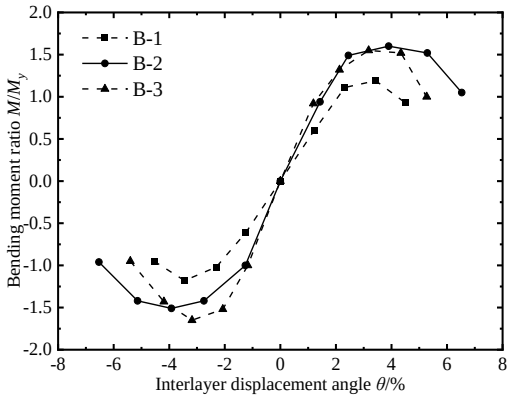

Fig. 6. M/M_y-θ Skeleton curves of specimens.

Energy consumption is reflected in the enclosed area of hysteresis curve with the bending moment M and displacement angle θ. A regularized energy consumption index, I_{ni}, is used to describe the energy consumption efficiency of the overall hysteresis process, as shown in the Eq. (1).

$$I_{ni} = \int (M_{ni}\,\theta_{ni})d\theta \big/ (M_y\,\theta_y) \tag{1}$$

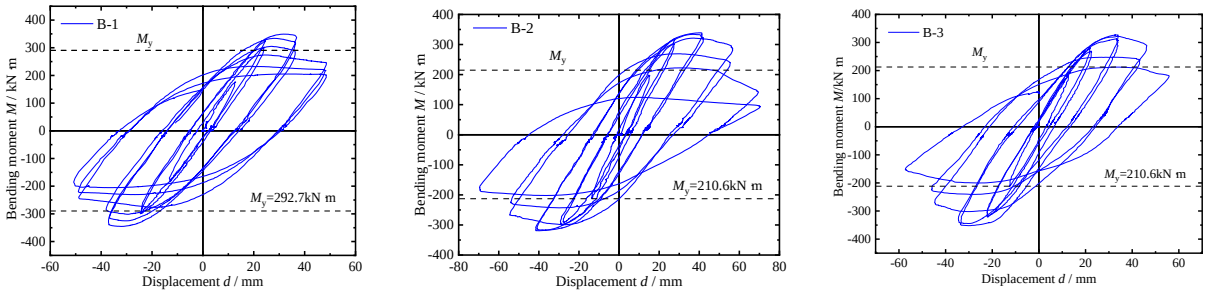

(a) Specimen B-1 (b) Specimen B-2 (c) Specimen B-3

Fig. 7. *M-d* Hysteretic loops of box-section columns.

Note:
M_{ni} —Bending moments by the *n*-loading level and *i*-circle of hysteresis curve; θ_{ni}—corresponding inter-story drift angle by the n-loading level and i-circle of hysteresis curve
M_y — Yield bending moment of the component section; θ_y — Inter-story drift angle corresponding to M_y

The results of the energy consumption index Ini are shown in Fig. 8. Comparing B-1 and B-2, it can be seen that the width-to-thickness ratio of the plate has an influence on the energy dissipation capacity. The larger the width-thickness ratio is, the earlier it enters the local buckling state, which makes the bearing capacity and the energy dissipation capacity decrease. Comparing B-2 and B-3, it can be seen that under the gravity second-order effect, the large deformation causeed by the axial pressure makes the ductility decrease, which leads to the reduction of energy consumption.

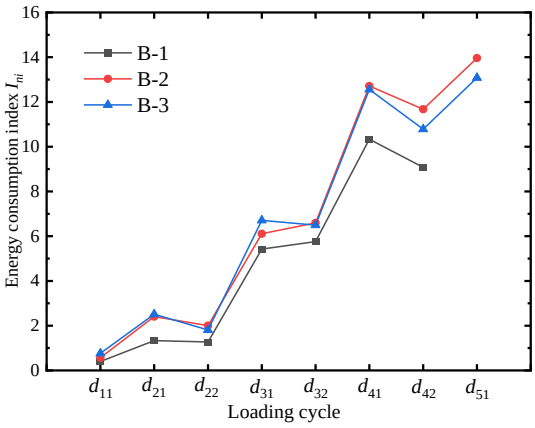

Fig. 8. Energy consumption index I_{ni} chart.

The damage assessment of the specimens is mainly characterized by the damage index *D*. The index *D* is increasing between 0 and 1, which indicates the process of accumulating damage to the specimen until it is destroyed. It shows the irreversibility and non-directional characteristics of the damage. *D* expresses as shown in Eq. (2).

$$S_i = S_0 \cdot (1 - D) \tag{2}$$

S_i is each state of the specimen and S_0 is the initial state. The damage index *D* is calculated with reference to the equation proposed by Hwang [9]. Hwang integrated the changes of deformation, energy and bearing capacity during the hysteresis process and combined the products by different weighting factors. With each parameter taken as 1, the most significant influencing factor on the damage is the deformation of member, followed by the change in energy consumption and finally the decay of the bearing capacity. The calculation formula and related parameters are expressed in Eq. (3).

$$D = \sum_{i=1}^{n} (\mu_{si} - 1)^{\varphi} \cdot \lambda_i \cdot \alpha_i \tag{3}$$

Note:
$\mu_{si} = S_i / S_y$; S_i —Displacement corresponding to the i-th loading stage;
S_y—Yield displacement; P_y—Yield bearing;
$\alpha_i = E_i / (P_y S_y)$ — Percentage of hysteresis energy consumption of the i-th loading stage;
E_i—Hysteresis energy consumption of the i-th loading stage;
$\lambda = P_{ui} / P_y$; P_{ui}—Peak bearing capacity of the i-th loading stage.

The damage index *D* is calculated and corrected with *D*=1 at the time of failure. The damage variation curve of each specimen is plotted in Fig. 9 by taking the value of *D* as the vertical coordinate and the ratio of the current displacement loading level *n* to the total loading level *N* as the horizontal coordinate.

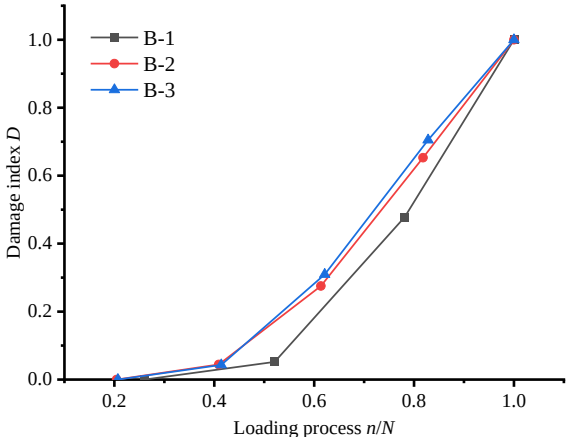

Fig. 9. Damage index-*D*.

The trend of the damage index D shows that the damage curve is concave, reflecting its characteristics of slow development in the early stage and fast growth in the later stage. Under the influence of bearing capacity, the damage development of specimens B-1 and B-2 is more smooth and continuous, and the damage of B-3 is close to 50% in the last loading level, showing its discontinuous characteristics. It can be seen that the width-to-thickness ratio has an influence on the continuity of damage development, and the smaller the plate width-thickness ratio is, the more continuous the damage development is.

C. Comparison of Existing Research

The seismic performance results of Q690D box-section column by Guoqiang Li [10] were selected for comparison. The excerpted specimen B-L and B-3 are designed according to the plastic section (S1, S2) and their axial compression ratio is the same. The length-to-slend ratio do not affect the local stability of columns, so it do not come into question. The mechanical properties of them are shown in the Table Ⅴ. It shows that the new steel Q620E has lower yield ratio and higher ultimate strain, and its material properties are better than those of Q690D high-strength steel. The dimensional information of the members is shown in Table VI, and the yield moment M_y is calculated based on the material properties and cross-sectional dimensions. As shown in Table VII, the new Q620E B-3 box-section column is better than Q690D B-L box-section column in terms of bearing capacity and ductility.

TABLE V. COMPARISON OF MATERIAL PROPERTIES

-	E/MPa	f_y/MPa	f_u/MPa	f_y/f_u	ε_u
Q620E	210286	655.1	761.9	0.86	0.0753
Q690D[6]	236900	779.0	834.00	0.93	0.0590

TABLE VI. DIMENSION INFORMATION OF COMPONENT

-	D/mm	t/mm	L_0/mm	h_0/t	λ	n
B-3	180	8	1060	20.5(S2)	30.3	0.35
B-L	250	16	2505	13.6(S1)	52.3	0.35

TABLE VII. COMPARISON OF COMPONENT TEST RESULTS

-	M_y	M_u/kN • m	M_u/M_y	θ_u/%rad
B-3	210.6	352.2	1.67	4.76
B-L	855.7	892.9	1.04	4.34

The comparison of the energy dissipation capacity of the specimens is shown in Fig. 10. B-3 is better than that of B-L after the elastic-plastic working stage. The comparison shows that the new Q620E steel has greater advantages over Q690D ordinary high-strength steel in terms of mechanical properties and seismic design of members.

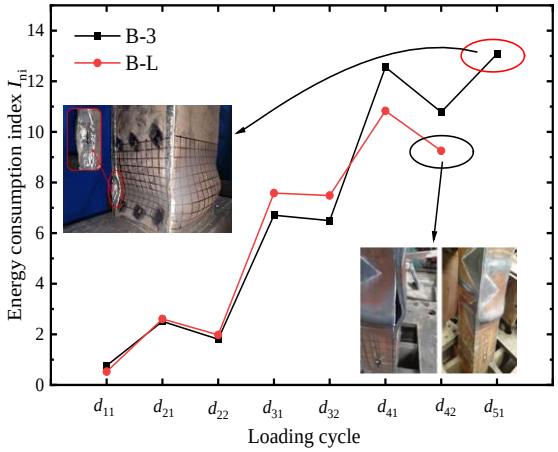

Fig. 10. Energy dissipation capacity of specimen B-3 and B-L.

IV. CONCLUSIONS

The analysis based on the results of the test is concluded as follows:

1) The Q620E steel meets the material requirements of the "Standard for design of high strength steel structure" and its yield ratio is about 0.85, which is lower compared to Q690D high-strength steel.

2) The failure mode of the box-section column is mainly the local instability of the specimen caused by the buckling of the wall plate. The smaller the width- thickness ratio of the plate is, the better the hysteresis performance of the member is, the higher the energy dissipation capacity is, the more continuously the damage development does.

3) The maximum inter-story drift angle of box-section column made of such steel is greater than 1/50, which meets the elastic-plastic angle limit of GB 50011–2010 "Code for seismic design of buildings".

4) Compared with Q690D ordinary high-strength steel, the new Q620E steel has greater advantages in terms of bearing capacity, ductility and energy dissipation capacity. It shows that the improved material properties may effectively improve the seismic performance. It may be considered for application in high-strength steel building structures.

CONFLICT OF INTEREST

The authors declare no conflict of interest.

AUTHOR CONTRIBUTIONS

Xiyu Ye wrote the original draft of the paper; Shidong Nie provided conceptualization and methodology; and Zhenye Chen reviewed and edited the manuscript; Cheng Ma and Jin Pan provided materials relevant data; all authors had approved the final version.

FUNDING

The authors would like to acknowledge the financial supports given through the Research, Design and

Application Project of Structural High-performance Steel of 690 MPa (Grant Project No. H20200688) and 111 Project (Grant No. B18062).

REFERENCES

[1] S. Gang, Y. J. Shi, Y. Q. Wang, "Engineering application of ultra-high strength steel structures," *Progress in Steel Building Structures*, vol. 04, pp. 32–38, 2008. (in Chinese)

[2] J. J. Wang, G. Shi, Y. J. Shi, "Experimental research on behavior of 460 MPa high strength steel I-section columns under cyclic loading," *Earthquake Engineering and Engineering Vibration*, vol. 13, no. 04, pp. 611–622, 2014. DOI: 10.1007/s11803-014-0267-4.

[3] S. W. Chen, X. Chen, Y. B. Wang, *et al*., "Experimental and numerical investigations of Q690D H-section columns under lateral cyclic loading," *Journal of Constructional Steel Research*, vol. 121, pp. 268–281, 2016. DOI: 10.1016/j.jcsr.2016.02.015

[4] L. T. Hai, G. Q. Li, Y. B. Wang, *et al.,* "Experimental investigation on cyclic behavior of Q690D high strength steel H-section beam-columns about strong axis," *Engineering Structures*, vol. 189, pp. 157–173, 2019. DOI: 10.1016/j.engstruct.2019.03.060

[5] Y. B. Wang, G. Q. Li, W. Cui, *et al.*, "Seismic behavior of high strength steel welded beam-column members," *Journal of constructional Steel*, vol. 102, pp. 245–255, 2014. DOI: 10.1016/j.jcsr.2014.07.015

[6] L. T. Hai, G. Q. Li, Y. B. Wang, *et al*., "Experimental investigation on cyclic behavior of Q690D high strength steel H-section beam-columns about strong axis," *Engineering Structures*, vol. 189, pp. 157–173, 2019. DOI: 10.1016/j.engstruct.2019.03.060

[7] L. T. Hai, G. Q. Li, Y. B. Wang, *et al.*, "Hysteretic model of Q690 high-strength steel beam-columns considering cyclic deterioration," *Journal of Constructional Steel Research*, 2020, 106158.1-106158.19. DOI: 10.1016/j.jcsr.2020.106158

[8] Standard for design of high strength steel structure:JGJ/T 483-2020. Beijing: China Architecture & Building Press, 2020. (in Chinese)

[9] T. H. Hwang, C. F. Scribner, "Member cyclic response during various loadings," *Journal of Structural Engineering*, vol. 110, no. 3, pp. 477–489, 1984. DOI:10.1061 /(ASCE) 0733-9445

[10] S. W. Chen, Z. L. Lu, G. Q. Li, *et al.*, "Cyclic loading tests of Q690D high strength steel welded columns," *Journal of Building Structures*, vol. 35, no. 12, pp. 97–103, 2014.(in Chinese)